PFC/RR-81-18

DOE/ET/51013-16
UC20D

ICRF HEATING OF FED*

D.T. Blackfield, R.E. Potok,
D.R. Cohn, and L. Bromberg

Plasma Fusion Center
Massachusetts Institute of Technology
Cambridge, MA 02139

April 1981

*Supported by U.S. DOE Contract DE-AC02-ET78-51013

ABSTRACT

Both 1-D slab and cylindrical models are used to examine second and third harmonic ICRF heating of FED. The slab model, which divides the plasma into 1500 thin uniform slabs, uses a full-wave treatment to examine the effects of mode conversion. The RF power profile and the amount of energy absorbed per radial pass are also calculated. The 1-D cylindrical model uses WKB theory and is incorporated into a 1-D cylindrical multi-species time-dependent fluid code to examine the temporal behavior of ICRF and to estimate the RF power needed to heat FED. Both models use the full 3×3 hot plasma dispersion tensor. We find that heating at the second harmonic of deuterium, ($f = 55$ MHz) with $k_{\|} = 0.1\text{cm}^{-1}$ appears to be the most attractive scenario. Over 90% of the RF power is damped within one radial pass. Most of the power is deposited at the center in the ions. From the space-time results we find that 40 MW of RF power supplied for 500 ms will heat FED to operating temperatures assuming Alcator-type scaling.

Several tokamaks [1–3] have been heated using radio frequency waves at the Ion Cyclotron Range of Frequencies (ICRF) with heating efficiencies comparable to those of neutral beams. Multi-megawatt ICRF experiments are planned for PLT, TFR and Alcator C. Since megawatt level power supplies are now available and high powered ICRF heating experiments have been successful, we investigated the feasibility of using ICRF to heat FED.

A 1-D slab model with a full-wave treatment is first used to determine the spatial behavior of ICRF and the importance of mode conversion. Then a 1-D cyclindrical model using a WKB treatment is incorporated into a time-dependent fluid code to determine the amount of RF power needed. Both models assume a local RF dispersion relation. The full 3×3 hot plasma dispersion tensor is used to determine complex $k_{\perp}$ given real ω and $k_{\|}$ (fixed in radius) for both the fast magnetosonic and Ion Bernstein waves [4].

In the time-independent 1-D slab model [5] the plasma is divided into many (up to 1500) thin, uniform slabs lying in the yz plane with B_o in the z direction. The local dispersion relation is solved in each slab for four modes, a fast wave ($\pm k_{\perp f}$) and an Ion Bernstein wave ($\pm k_{\perp I.B.}$) which propagate in both directions. In each slab the RF wave field is the linear combination of the individual mode fields,

$$E = \sum_{i=1}^{4} E_m e^{ik_{\perp m} \cdot r}, \qquad B = \sum_{i=1}^{4} B_m e^{ik_{\perp m} \cdot r}. \tag{1}$$

The amplitude coefficients E_m and B_m are calculated from the total tangential E and B fields, which are continous across a slab interface. The boundary conditions for the two plasma edge slabs are determined by the launching conditions. For FED, we assumed that a fast wave is launched from the low field side. To find the

electric and magnetic fields, a large (4800 for 1200 slabs) set of complex equations is numerically solved using a band matrix solver. For accurate solutions $k_\perp \Delta x \ll 1$, where Δx is the slab width. Since $k_\perp$ for the Ion Bernstein wave becomes large near the plasma edge, only the central 200 cm of plasma width ($0 \leq r \leq 100$ cm) can be used in the analysis. We do not examine the antenna-plasma coupling problem. However, our region of analysis is wide enough to contain all of the ion and most of the electron heating zones.

After solving for the E and B fields, we can calculate the total radial Poynting flux

$$P = \frac{-c}{8\pi} Re(E \times H^*). \tag{2}$$

The change in P from the low to high field side gives an estimate of the amount of RF power absorbed per radial pass.

To calculate the amount of RF power absorbed by each species, we use the weak damping formula

$$P^s_{RF} = \omega E^* \cdot (\sum_m \underline{\underline{K}}^A_{m,s} \cdot E_m) \tag{3}$$

where $\underline{\underline{K}}^A$ is the anti-hermitian part of the dielectric tensor, m the mode, and s the species.

In Table 1 we list the assumed FED parameters. In Table 2 we summarize our results from the 1-D slab calculations for different RF frequencies. For a 50–50 D-T plasma, when $f = 22.5$ MHz, the ion-ion hybrid resonance is located at the plasma center. However, the fundamental resonances of deuterium (at 587 cm) and tritium (at 391 cm) are located near the plasma edges. Therefore, if fundamental deuterium or tritium, or ion-ion hybrid resonance heating is attemped, edge heating may occur.

The most attrative heating scheme appears to be second harmonic deuterium ($2f_{CD}$), third harmonic tritium ($3f_{CT}$) heating when $f = 55$ MHz. However, higher harmonic deuterium heating ($3f_{CD}$) also leads to strong ion absorbtion near the plasma center and using the higher frequency could reduce the launching structure size. Second harmonic tritium ($2f_{CT}$) can be used to selectively heat tritium near the plasma center if desired.

Figure (1) shows the RF dispersion relation for both the fast and Ion Bernstein waves when $f = 55$ MHz at $t = 0.0$ ms with parabolic density and temperature profiles. At $t = 0.0$ ms, Fig. (2) shows that almost 94% of the incident RF is absorbed in one radial pass. At the time the RF is turned off at $t = 500$ ms, the hotter plasma temperatures produce nearly 100% absorption in one radial pass. Figure (3) shows that nearly 86% of the RF power is absorbed by the deuterons at the plasma center where the second harmonic resonance occurs. Figure (4) shows that only 1% of the RF power is absorbed directly by the tritons. The remaining RF power

(~ 14%) is absorbed by the electrons through Landau and transit time damping as shown in Fig. (5). The very small amounts of negative RF power absorption shown in Figs. (4–5) result from the slight inaccuracy of the weak damping formulation. In this case, second harmonic damping is strong.

Our 1-D slab calculations show that mode conversion does not seem to play an important role. Over 98% of the total RF heating results from the incident fast wave. In addition, since the fast wave wavelength is large compared to the scale length of plasma parameter changes, a WKB treatment of fast wave heating should be accurate. Consequently, we used a 1-D cylindrical WKB model connected to a 1-D multi-species, time-dependent fluid code [6] to examine the temporal behavior and determine the amount of ICRF power needed. Again Eq. (3) is used to calculate the amount of RF power going to each species with $m = 1$ since only the incident fast wave from the low field side has significant amplitude. The electric field is taken to have the following WKB form [6–7]

$$E \quad a \quad \frac{1}{k_{\perp f}^{1/2}} e^{i \int k_{\perp f} \cdot dr}. \tag{4}$$

From this code, we find that 40 MW supplied for 500 ms is enough power for FED to reach operating conditons assuming Alcator-type scaling [6]. Figures (6–7) show the temporal behavior of the ion and electron temperatures. Figures (8–9) show the RF power deposited in the ions and electrons averaged over the flux surfaces. As the plasma is heated, the ion heating zone spreads out and begins to shift toward the low field side. In addition, the amount of RF power deposited in the electrons increases.

1-D slab model results are again shown in Figs. (10–12). In this case, we have used the ion and electron temperature profiles at $t = 500$ ms as determined by the space-time RF code. Figure (10) shows that the heating zone has spread, as determined from $Im(k_{\perp f})^2$. This greatly enlarged heating zone produces essentially complete absorption of the RF in one radial pass. Figures (11–12) show that the amount of electron absorption increased to 36% while second harmonic absorption decreased to 61% . The remaining 3% is deposited in the tritons over the region $0 \leq r \leq 26$ cm. Even with the spreading and shifting of the heating zone, both the ion and electron temperatures remain center-peaked.

We conclude that for a 50–50 D-T FED-type plasma, 40 MW of ICRF power for 500 ms with $f \approx 55$ MHz (corresponding to second harmonic deuterium and third harmonic tritium heating) would be needed, assuming Alcator scaling. The absorption is peaked toward the center with the ions receiving more than 85% of the incident power. The absorption is quite strong with more than 94% of the incident fast wave power absorbed in one radial pass. Mode conversion should not play a significant role. Over 98% of the RF heating comes from the incident fast wave launched from the low field side.

Table 1

FED Parameters

R_o (cm)	$= 480$
a (cm)	$= 130$
$n_D(0) = n_T(0)$ (cm)	$= 7.8 \times 10^{13}$
n_D (edge) $= n_T$ (edge) (cm)	$= 7.8 \times 10^{12}$
B_o (kG)	$= 36.2$

	at $t = 0.0$ ms	at $t = 500$ ms
$T_i(0)$ (keV)	$= 2.0$	33
$T_e(0)$ (keV)	$= 2.0$	25
$\overline{T}_i$ (keV)	$= 1.0$	6.7
$\overline{T}_e$ (keV)	$= 1.0$	5.3

RF Parameters

P_{RF} (MW)	40
$k_{\|}$ (cm^{-1})	0.1
a (1-D slab model) (cm)	100
Δx (1-D slab model) (cm)	0.2
t_{RF} (space-time model) (ms)	500

Table 2

Summary of 1-D Slab Model Results

Harmonic	f	ΔP	P^E_{RF}	P^D_{RF}	P^T_{RF}
	MHz	%	%	%	%
$2f_{CT}$	36.7	42	55.9		44.0
$3f_{CD}$	82.5	30	17.2	74.3	8.5*
$2f_{CD} = 3f_{CT}(f = 0.0$ ms)	55	94	13.5	85.8	0.7
$2f_{CD} = 3f_{CT}(t = 500$ ms)	55	100	35.8	61.0	3.2

* When $f = f_{CD} = 82.5$ MHz at 480 cm, the fourth harmonic of tritium ($f = 4f_{CT}$) is at r = 427 cm.

Figures

Fig. 1. Real (solid lines) and imaginary (dashed lines) parts of $(k_x^2)^{1/5}$ for both the fast (f) and Ion Bernstein (I. B.) waves for parabolic temperature and density profiles at $t = 0.0$ ms with $f = 55$ MHz and $k_{||} = 0.1$ cm^{-1}.

Fig. 2. Radial Poynting flux (P_x) at $t = 0.0$ ms. The negative value indicates propagation from the low field side. The slope indicates strength of absorption. The gradual slope at the low field side, caused by electric Landau and transit time damping, gives way to the strong ion absorption at the center.

Fig. 3. RF power to deuterium at $t = 0.0$ ms (85.8% of total RF power).

Fig. 4. RF power to tritium at $t = 0.0$ ms (~ 1% of total RF power).

Fig. 5. RF power to electrons at $t = 0.0$ ms (13.5% of total RF power). The much smaller values on the higher field side again indicate that the ion absorption at the center is very strong and the wave energy which tunnels through is greatly reduced.

Fig. 6. Time-dependent electron temperature determined using Alcator scaling from the 1-D fluid code using 40 MW of RF power for 500 ms.

Fig. 7. Time-dependent ion temperature.

Fig. 8. Time-dependent electron heating RF profile. The heating increases and shifts toward the low field side due to the increasing electron Landau and transit time damping.

Fig. 9. Time-dependent ion heating RF profile. The ion heating zone spreads out and shifts toward the low field side as the temperature increases. However, both the electron and ion temperatures remain center-peaked.

Fig. 10. Real (solid lines) and imaginary (dashed lines) parts of $(k_x^2)^{1/5}$ for both the fast (f) and Ion Bernstein (I. B.) waves at $t = 500$ ms.

Fig. 11. RF power to deuterium at $t = 500$ ms (61.0% of total RF power).

Fig. 12. RF power to electrons at $t = 500$ ms (35.8% of total RF power).

References

1. J. Hosea *et al*, Princeton University Plasma Physics Laboratory Report PPPL–1588 (Oct. 1979).
2. TFR Group in Controlled Fusion and Plasma Physics Research (Proc. 9th European Conf., Oxford, Sept. 1979).
3. Haruyuki Kimura *et al*, Japan Atomic Energy Research Institute Report JAERI-M 8429 (Sept. 1979).
4. D. G. Swanson, Phys. of Fluids 10 (1967) 428.
5. D. T. Blackfield, B. D. Blackwell, M. Sansone, and M. Porkolab, Bull. Am. Phys. Soc. 25 (1980) 905; B. D. Blackwell and D. T. Blackfield, 4th Topical Conf. on RF Heating in Plasma (Austin, Texas, Feb. 1981) Paper A13.
6. D. T. Blackfield, University of Wisconsin-Madison Report UWFDM-353 (May 1980).
7. B. McVey, University of Wisconsin-Madison Report PLP 755 (May 1978).

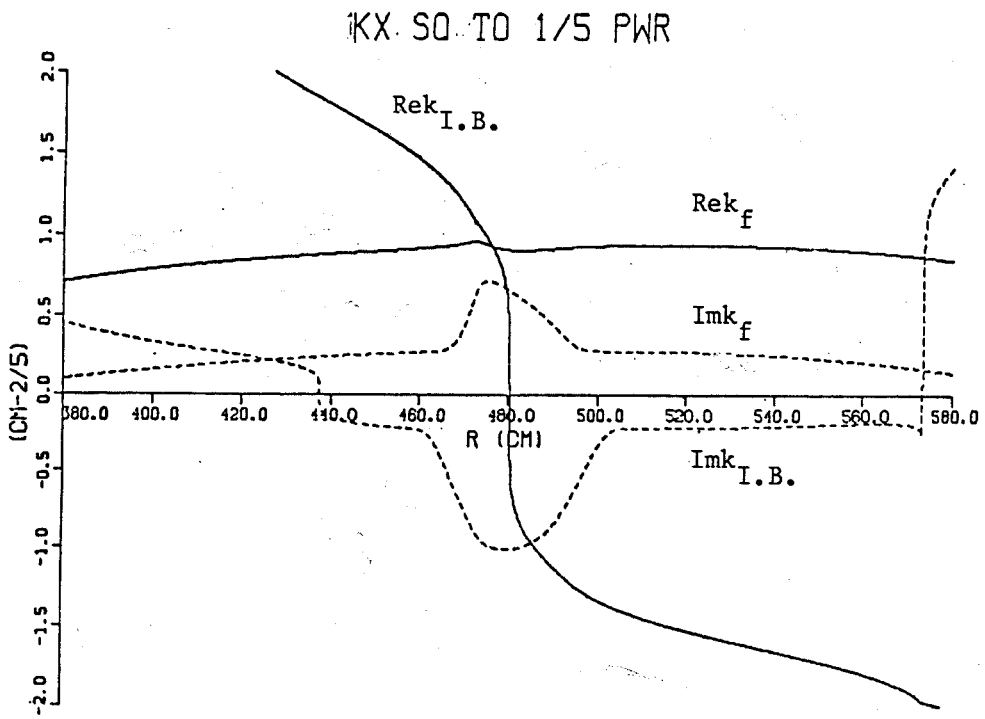

Figure 1

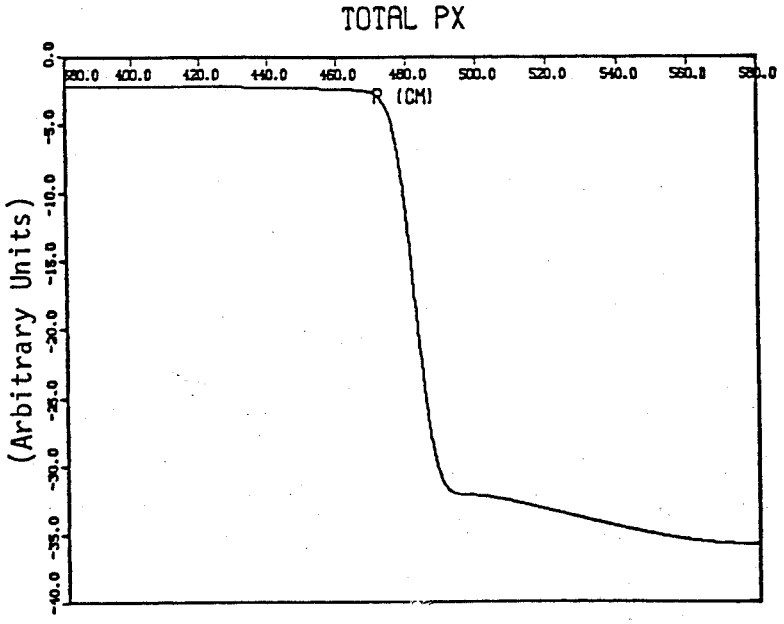

Figure 2

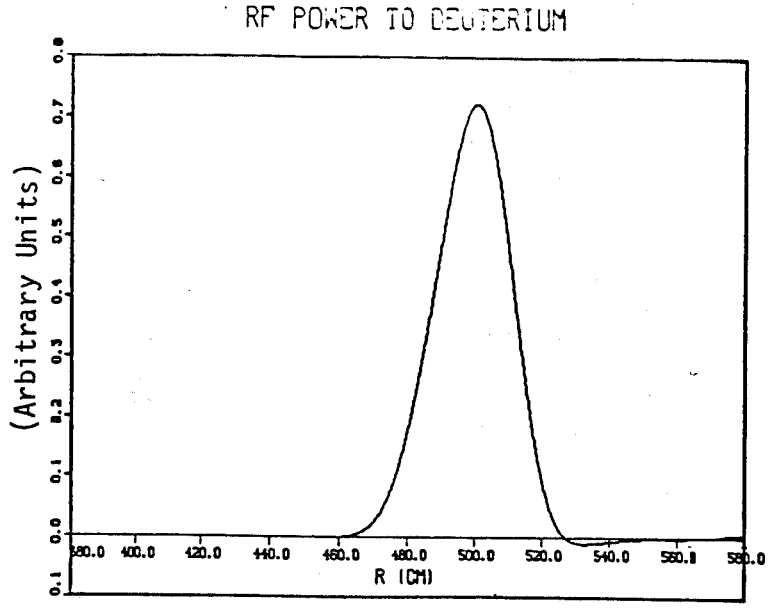

Figure 3

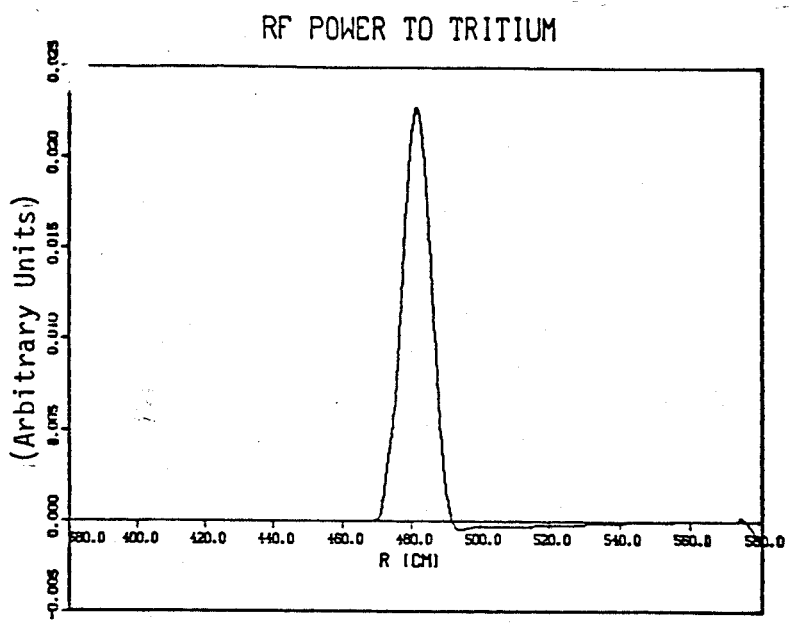

Figure 4

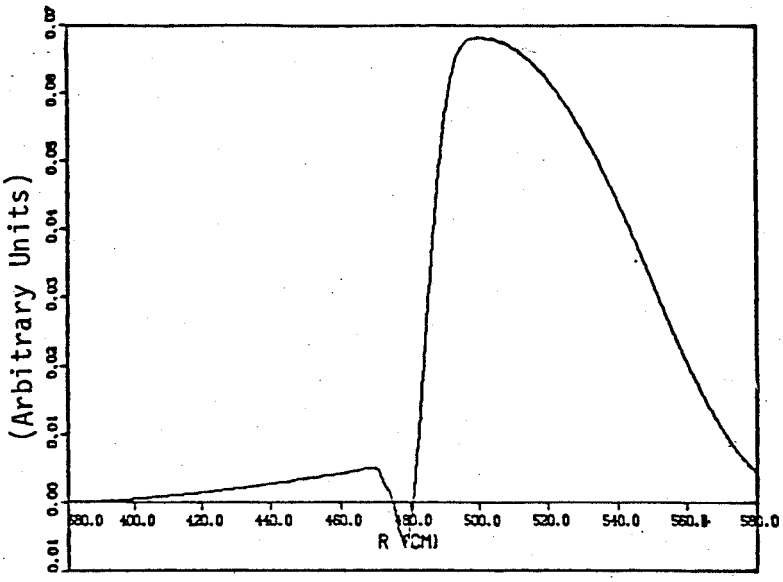

Figure 5

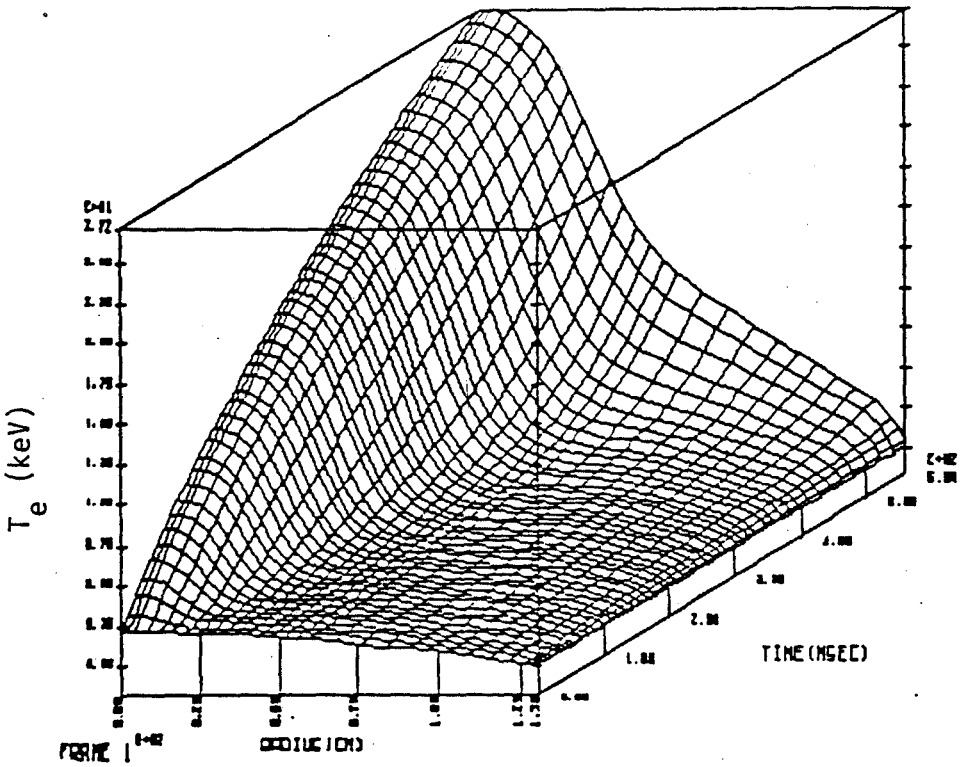

Figure 6

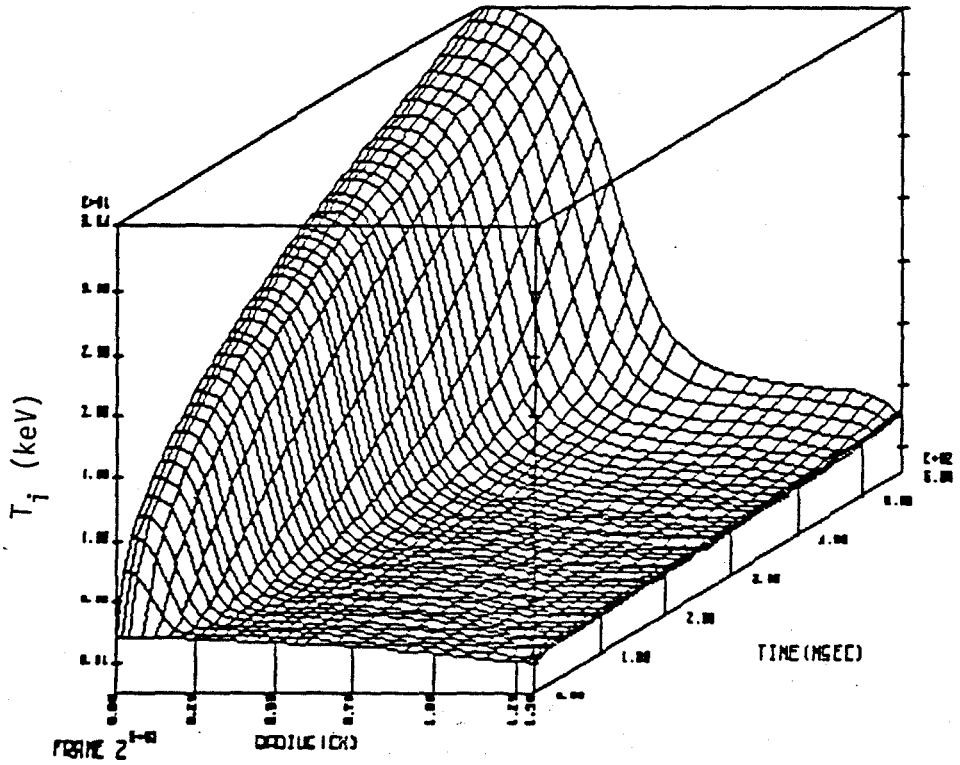

Figure 7

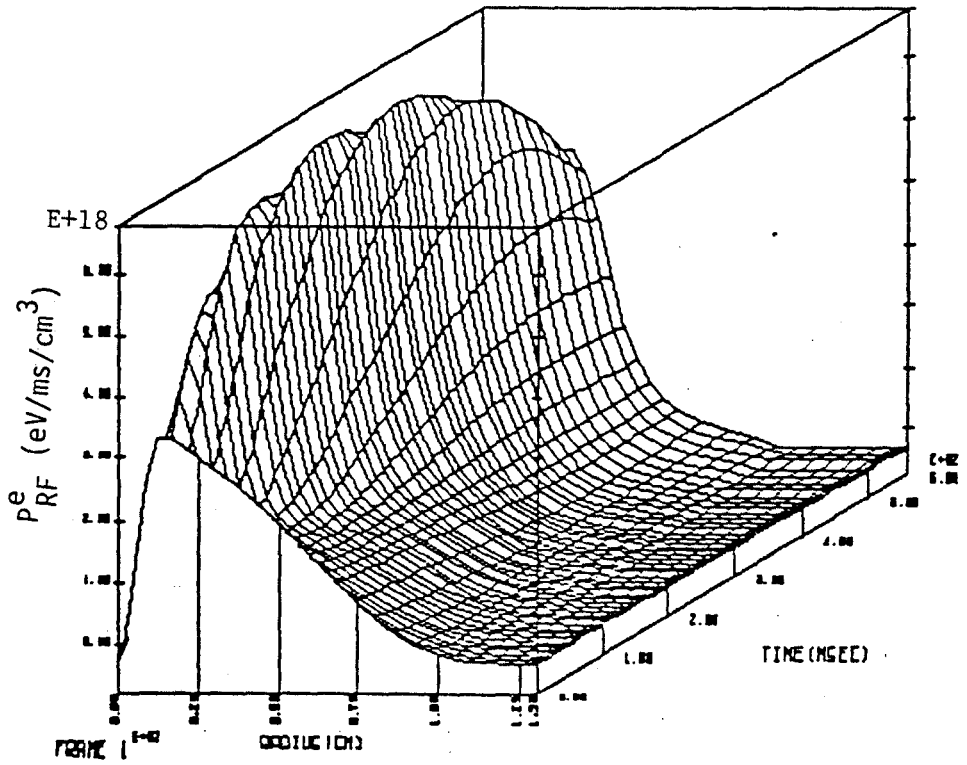

Figure 8

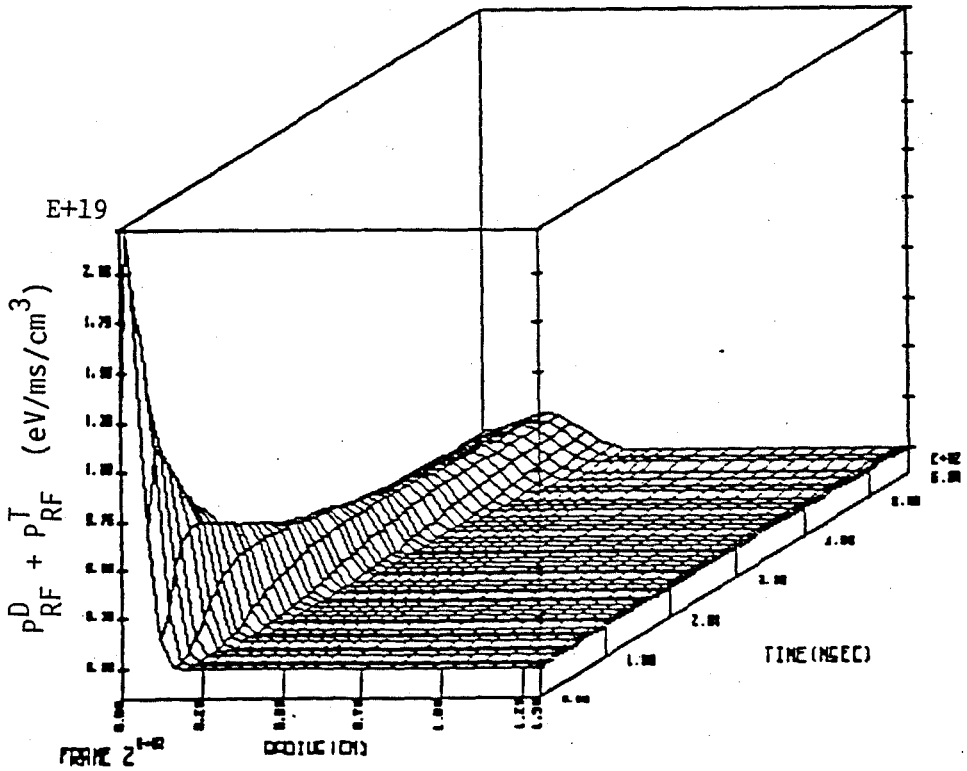

Figure 9

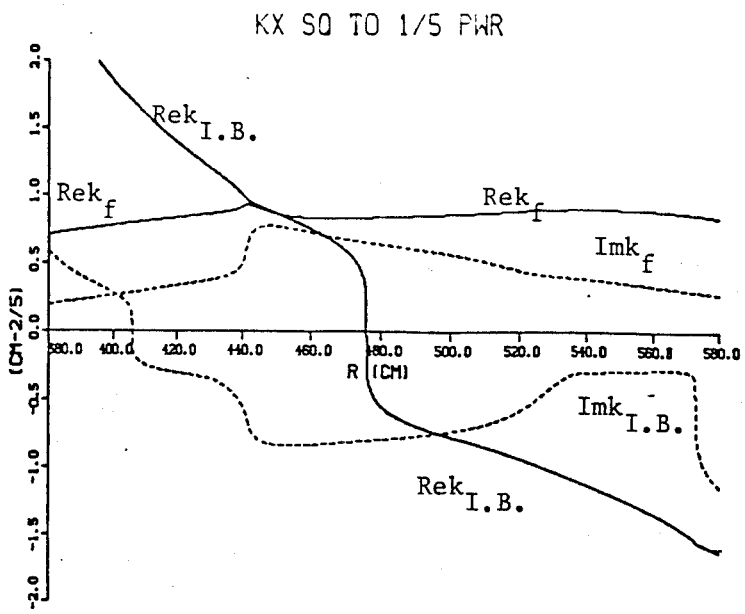

Figure 10

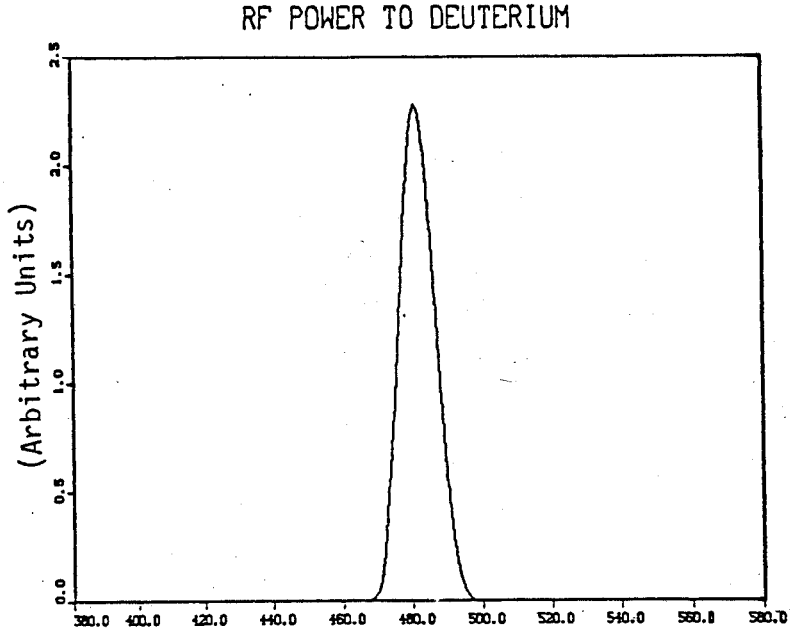

Figure 11

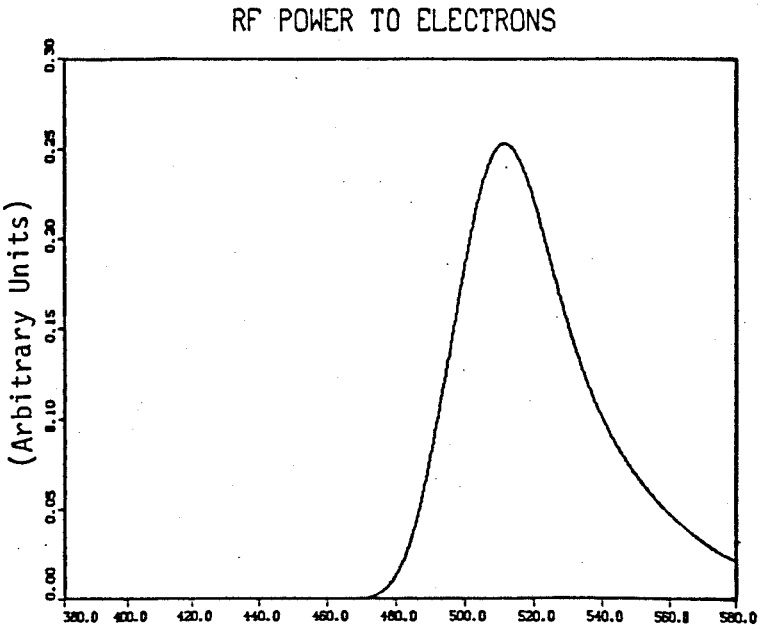

Figure 12

PFC BASE LIST

INTERNAL MAILINGS (MIT)

G. Bekefi
36-213

A. Bers
38-260

D. Cohn
NW16-250

B. Coppi
26-201

R.C. Davidson
NW16-202

T. Dupree
38-172

S. Foner
NW14-3117

J. Freidberg
38-160

A. Gondhalekar
NW16-278

M.O. Hoenig
NW16-176

M. Kazimi
NW12-209

L. Lidsky
38-174

E. Marmar
NW16-280

J. McCune
31-265

J. Meyer
24-208

D.B. Montgomery
NW16-140

J. Moses
NE43-514

D. Pappas
NW16-272

R.R. Parker
NW16-288

N.T. Pierce
NW16-186

P. Politzer
NW16-286

M. Porkolab
36-293

R. Post
NW21-

H. Praddaude
NW14-3101

D. Rose
24-210

J.C. Rose
NW16-189

R.M. Rose
4-132

B.B. Schwartz
NW14-5121

R.F. Post
NW21-203

L.D. Smullin
38-294

R. Temkin
NW16-254

N. Todreas
NW13-202

J.E.C. Williams
NW14-3210

P. Wolff
36-419

T.-F. Yang
NW16-164

Industrial Liaison Office
ATTN: Susan Shansky
Monthly List of Publications
39-513

MIT Libraries
Collection Development
ATTN: MIT Reports
14E-210

B. Colby
PFC Library
NW16-255

EXTERNAL MAILINGS

National

Argonne National Laboratory
Argonne, IL 60439
ATTN: Library Services Dept.

Battelle-Pacific Northwest Laboratory
P.O. Box 99
Richland, WA 99352
ATTN: Technical Information Center

Brookhaven National Laboratory
Upton, NY 11973
ATTN: Research Library

U.S. Dept. of Energy
Washington, D.C. 20545
ATTN: D.O.E. Library

Roger Derby
Oak Ridge National Lab.
ETF Design Center
Bldg. 9204-1
Oak Ridge, TN 37830

General Atomic Co.
P.O. Box 81608
San Diego, CA 92138
ATTN: Library

Lawrence Berkeley Laboratory
1 Cyclotron Rd.
Berkeley, CA 94720
ATTN: Library

Lawrence Livermore Laboratory
UCLA
P.O. Box 808
Livermore, CA 94550

Oak Ridge National Laboratory
Fusion Energy Div. Library
Bldg. 9201-2, ms/5
P.O. Box "Y"
Oak Ridge, TN 37830

Dr. D. Overskei
General Atomic Co.
P.O. Box 81608
San Diego, CA 92138

Princeton Plasma Physics Laboratory
Princeton University
P.O. Box 451
Princeton, NJ 08540
ATTN: Library

Plasma Dynamics Laboratory
Jonsson Engineering Center
Rensselaer Polytechnic Institute
Troy, NY 12181
ATTN: Ms. R. Reep

University of Wisconsin
Nuclear Engineering Dept.
1500 Johnson Drive
Madison, WI 53706
ATTN: UV Fusion Library

EXTERNAL MAILINGS

International

Professor M.H. Brennan
Willis Plasma Physics Dept.
School of Physics
University of Sydney
N.S.W. 2006, Australia

Division of Plasma Physics
Institute of Theoretical Physics
University of Innsbruck
A-6020 Innsbruck
Austria

c/o Physics Section
International Atomic Energy Agency
Wagramerstrasse 5
P.O. Box 100
A-1400 Vienna, Austria

Laboratoire de Physique des Plasmas
c/o H.W.H. Van Andel
Dept. de Physique
Universite de Montreal
C.P. 6128
Montreal, Que H3C 3J7
Canada

Plasma Physics Laboratory
Dept. of Physics
University of Saskatchewan
Saskatoon, Sask., Canada S7N OWO

The Library
Institute of Physics
Chinese Academy of Sciences
Beijing, China

Mrs. A. Wolff-Degives
Kernforschungsanlage Julich GmbH
Zentralbibliothek - Exchange Section
D-5170 Julich - Postfach 1913
Federal Republic of Germany

Preprint Library
Central Research Institute for Physics
H-1525 Budapest, P.O. Box 49
Hungary

Plasma Physics Dept.
Israel Atomic Energy Commission
Soreq Nuclear Research Center
Yavne 70600
Israel

The Librarian (Miss DePalo)
Associazione EURATOM - CNEN Fusione
C.P. 65-00044 Frascati (Rome)
Italy

Librarian
Research Information Center
Institute of Plasma Physics
Nagoya University
Nagoya, 464
Japan

Dr. A.J. Hazen
South African Atomic Energy Board
Private Bag X256
Pretoria 0001
South Africa